Synthesis and Magnetic Properties of Biocompatible Hybrid Hollow Spheres

Yin Ding,[†] Yong Hu,[†] Leyang Zhang,[†] Ying Chen,[†] and Xiqun Jiang*[,†,‡]

Lab of Mesoscopic Chemistry and Department of Polymer Science and Engineering, College of Chemistry and Chemical Engineering and Jiangsu Provincial Laboratory for Nanotechnology, Nanjing University, Nanjing, 210093, China

Received January 27, 2006; Revised Manuscript Received April 9, 2006

Magnetic hybrid hollow spheres of about 200 nm were prepared by a core-template-free route, that is, adding Fe_3O_4 nanoparticles stabilized by poly(vinyl alcohol) (PVA) to an aqueous solution of polymer−monomer pairs composed of a cationic polymer, chitosan (CS), and an anionic monomer, acrylic acid (AA), followed by polymerization of acrylic acid and selective cross-linking of chitosan at the end of polymerization. The obtained hybrid spheres were characterized by dynamic light scattering (DLS) in aqueous solution and observed by transmission electron microscopy (TEM), scanning electron microscopy (SEM), and atomic force microscopy (AFM) in the solid state. Fourier transform infrared spectroscopy (FTIR) and X-ray and electron diffractions revealed that the Fe_3O_4 nanoparticles were incorporated into the shells of chitosan−poly(acrylic acid) (CS−AA) hollow spheres. Magnetization studies and Mössbauer spectroscopy suggested that the chains (or islands) of iron oxide nanoparticles were most likely formed in the walls of the hollow spheres. The phantom test of magnetic resonance imaging showed that the synthesized hybrid hollow spheres had a significant magnetic resonance signal enhancement in T2-weighted image.

Introduction

Assembly of inorganic components into polymeric capsules or hollow spheres has received increasing attention due to combination of the properties of inorganic and organic components, thereby making them ideal candidates for applications ranging from targeting drug delivery, catalysis carriers, to bioseparation and diagnostic contrast agents.[1,2] Currently, a widely used approach for the synthesis of organic−inorganic hybrid hollow spheres is a core-template-based strategy in which the inorganic components are coated on the polymer-templating particles by sol−gel chemistry[3] or layer-by-layer deposition.[4] One advantage of such an approach is that the thickness of the coating layers is controllable. While successful and flexible, this approach requires sacrificial core templates and needs to remove the core to create a hollow structure. Hence, development of a core-template-free strategy for fabrication of hollow hybrid spheres is an interesting subject. Stucky and co-workers reported a room temperature, wet chemical-based synthesis route in which silica and gold nanoparticles are cooperatively assembled with lysine−cysteine diblock copolypeptides into micrometer-sized hybrid hollow spheres without the use of a sacrificial core and hollow preformed substrate.[5] In an extension of their work, Cha, Stucky, and co-workers very recently showed that positively charged poly(L-lysine) and negatively charged Au, CdSe, and SiO_2 nanoparticles can assemble into micrometer-sized composite hollow spheres using homopolymer, poly(L-lysine).[6] Du and Chen showed that the organic/inorganic hybrid hollow particles can be prepared by assembly of reactive diblock copolymer containing trimethyloxysilyl moieties in mixed solvents.[7] Besides these assembly routes, liquid-phase deposition of inorganic nanoparticles on polymeric capsules, impregnation of the capsules with preformed inorganic nanoparticles, and selective synthesis of inorganic nanoparticles inside the polyelectrolyte capsules were also reported.[8,9]

Since magnetic nano- or microparticles of iron oxides have wide application in biomedical and diagnostic fields, including separation of biochemical products,[10] gene manipulation and immunoassay,[11] enzyme immobilization,[12] magnetic resonance imaging (MRI) contrast agents,[13] and magnetically guided site-specific drug delivery agents,[14] it is of interest to construct magnetic Fe_3O_4−polymer hollow spheres with a core-template-free route using biocompatible and biodegradable materials. In our previous communication, we reported the preparation of hybrid hollow nanospheres with a size of less than 100 nm.[15] However, the magnetic properties and magnetic resonance (MR) signal-enhancement effect of Fe_3O_4–polymer hollow spheres are unprecedented. Since the properties of hybrid spheres are strongly influenced by their size, it is interesting to explore the synthesis and properties of hybrid hollow spheres with a distinct size difference. In this article, we extend our work to the synthesis of magnetic hybrid hollow spheres with a larger size and investigation of the magnetic properties and ability of MR signal enhancement of magnetic Fe_3O_4/chitosan−poly(acrylic acid) hybrid hollow spheres.

Experimental Section

Materials. Chitosan (CS; Nantong Shuanglin Biological Product Inc.) was refined twice as follows. First, chitosan was dissolved in dilute acetic acid solution, and the solution was filtered. Then the filter liquor was poured into an aqueous NaOH solution to precipitate CS, followed by washing with distilled water. Finally, the CS was dried in a vacuum at room temperature for use. The deacetylation degree of CS was about 90%, and the weight-average molecular weight of CS was 200 KDa, determined by viscometric methods. Potassium persulfate ($K_2S_2O_8$) was

* To whom correspondence should be addressed. Fax: +86 25 83317761. E-mail: jiangx@nju.edu.cn.

[†] College of Chemistry and Chemical Engineering.

[‡] Jiangsu Provincial Laboratory for Nanotechnology.

10.1021/bm060085h CCC: $33.50
Published on Web 05/11/2006

recrystallized from distilled water. Acrylic acid (AA) (Shanghai Guanghua Chemical Co.) was distilled under reduced pressure in a nitrogen atmosphere. Poly(vinyl alcohol) (PVA, AIRVOL 540) was purchased from Air Products and Chemicals Inc. Iron(II) chloride tetrahydrate (99%), iron(III) chloride hexahydrate (97%), sodium hydroxide, and glutaraldehyde (GA, 25% aqueous solution) were used as received without further purification.

Synthesis of Fe_3O_4 Nanoparticles. The Fe_3O_4 nanoparticles stabilized by poly(vinyl alcohol) (PVA) were synthesized according to the method described by Lee[16] with some modification. Briefly, a mixed aqueous solution containing 0.5 M Fe(II) and 0.5 M Fe(III) was prepared with $FeCl_2 \cdot 4H_2O$ and $FeCl_3 \cdot 6H_2O$. Then, the iron ion mixed solution was ultrasonically dispersed in an equal volume of PVA aqueous solution (2 wt %), and the pH of the solution was adjusted to 11 by addition of sodium hydroxide solution (5 M). The reaction system was sonicated for 5 min and stirred for 2 h at room temperature. After that, the product was filtered and dialyzed against the distilled water in order to remove unreacted iron and chlorate ions. Finally, a PVA-stabilizing magnetite nanoparticle suspension ($\sim 1 \times 10^{16}$ Fe_3O_4 particles/mL) was obtained.

Synthesis of Fe_3O_4/CS−PAA Hollow Spheres. A 0.25 g amount of CS was dissolved in 60 mL of AA aqueous solution in a ratio of 1.1:1 ([aminoglucoside unit in CS]:[AA]) under mechanical stirring. Until the solution became clear, 10 mL of PVA-stabilized magnetite nanoparticle suspension was added to the CS−AA solution. The polymerization reaction of AA was initiated by $K_2S_2O_8$, and the reaction was allowed to proceed for 2 h at 353 K under a nitrogen atmosphere. After the reaction system was cooled to 313 K, 0.2 mL of 25% GA aqueous solution was added to this reaction system to cross-link CS, and the cross-linking reaction was allowed to proceed for 2 h. Lastly, the resulting product was filtered to remove any possible aggregation. The unloaded magnetite nanoparticles were separated by three or more consecutive cycles whereby the suspension was ultracentrifuged (Ultra Pro 80, 8000 r min^{-1}, 277 K), the supernatant was discarded, and the wet solid was resuspended in water.

Characterization. The hydrodynamic diameter and size distribution of the prepared Fe_3O_4 nanoparticles and Fe_3O_4 nanoparticle-loaded CS−PAA hollow spheres were determined by dynamic light scattering (DLS) using a Brookhaven BI9000AT system (Brookhaven Instruments Corp.). All measurements were repeated 3 times with a wavelength of 658.0 nm. The zeta potential of the samples was obtained with Zetaplus (Brookhaven Instruments Corp.). Each sample was adjusted to a concentration of 0.1% (wt/v) in 0.1 M NaCl solution. All analyses were done in triplicate, and the results were the average of three runs.

FTIR spectra were recorded on a Bruker IFS66V spectrometer to analyze the interaction between CS and PAA, PAA and PVA, as well as Fe_3O_4 and PVA. The powder samples were prepared by lyophilizing, and measurements were carried out in a vacuum.

Wide-angle X-ray diffraction (WAXD) patterns of Fe_3O_4 nanoparticles and Fe_3O_4 nanoparticle-loaded CS−PAA hollow spheres were recorded on a Rigaku D/Max-Ra X-ray diffractometer employing Ni-filtered Cu Kα radiation (30 KV, 50 mA) at room temperature. The scanning rate was 0.04 deg s^{-1}.

Thermogravimetric analysis (TGA) measurements were performed with a thermal analyzer (TAC71DX, Perkin-Elmer) under N_2 at a temperature range of 293−900 K. The heating rate was 20 K min^{-1}.

Transmission electron microscopy (TEM, JEOL TEM-100, Japan) was used to observe the morphology of the Fe_3O_4 nanoparticles and Fe_3O_4 nanoparticle-loaded CS−PAA hollow spheres. Samples were placed onto a copper grid covered with nitrocellulose, dried at room temperature, and then examined using TEM without staining. For microtoming samples, an aqueous suspension of the Fe_3O_4 nanoparticle-loaded CS−PAA hollow spheres was frozen at −80 °C for 24 h, and then the sample was lyophilized to dry powder. A few granules of the resulting powder were embedded in epoxy resin, and sections of about 70 nm thick were obtained by microtoming the resin sample at room temperature.

Scanning electron micrographs (SEM) of hybrid hollow spheres were obtained with a JEOL JSM 6360 instrument. To avoid charging, all samples were sputter-coated with gold. The operating voltage was set at 10 or 20 kV.

Atomic force microscopy (AFM) (SPI3800, Seiko Instruments Inc, Japan) was used to study the surface morphology of spheres. One drop of properly diluted sample was placed on the surface of a clean silicon wafer and dried under nitrogen flow at room temperature. The AFM observation was performed with a 20-μm scanner in tapping mode.

Magnetic measurements were carried out in a vibrating sample magnetometer (VSM model 1660 digital system Inc.).

Mössbauer experiments were carried out using a ^{57}Co/Pd source in a constant-acceleration transmission spectrometer. The spectrum was recorded at room temperature. The spectrometer was calibrated using a standard α-Fe foil, and the reported isomer shifts (I.S.) were relative to the center of the α-Fe spectrum. The MossWinn program was used to determine the Mössbauer parameters.

Magnetic resonance imaging (MRI) was performed on a 1.5T superconducting magnet scanner (Gyroscan Intera Master, Philips, Netherlands) with a T2-weighted spin−echo sequence. Image parameters included TR/TE = 3000 ms/80 ms, field of view (FOV) = 20 × 20 cm, acquisition matrix = 256 × 256, receiver bandwidth (RBW) = 16 kHz, and slice thickness = 2 mm.

For FT-IR, XRD, TGA, VSM, and Mössbauer measurements the dried samples were prepared by lyophilizing to dry powder.

Results and Discussion

Synthesis of Fe_3O_4 Nanoparticle/Chitosan−Poly(acrylic acid) Hollow Spheres. Preparation of the hybrid magnetic hollow spheres was achieved by adding PVA-stabilized Fe_3O_4 nanoparticles to the aqueous solution of polymer−monomer pairs composed of a cationic polymer, chitosan (CS), and an anionic monomer, acrylic acid (AA). We chose PVA to stabilize Fe_3O_4 nanoparticles based on the following reasons: (1) PVA can interact with poly(acrylic acid) (PAA) by formation of a hydrogen bond between them,[17] which may result in the incorporation of PVA-stabilized Fe_3O_4 nanoparticles into CS−PAA hollow spheres; (2) The changes of pH and ionic strength have little effect on the PVA because of its acid and basic stability. Thus, after addition of Fe_3O_4 nanoparticles into CS−AA aqueous solution, followed by polymerization of AA monomer, and selectively cross-linking CS using glutaraldehyde at the end of polymerization, the Fe_3O_4 nanoparticle-loaded CS−PAA spheres were prepared. The size of the hollow sphere can be adjusted by controlling the concentration of chitosan−acrylic acid assemblies in the reaction system and the amount of cross-linker added.[18] The obtained suspension was filtered to remove any possible aggregation. The unloaded magnetite nanoparticles were separated by three or more consecutive cycles whereby the suspension was ultracentrifuged, the supernatant was discarded, and the wet solid was resuspended in water. Figure 1 shows the size distribution of synthesized hybrid spheres measured by dynamic light scattering before and after ultracentrifugation treatment. It can be seen that the size distribution of the sample before treatment is a bimodal size distribution: a dominant peak at about 200 nm and a minor peak around 9 nm. Compared with the size distribution of synthesized PVA-stabilized Fe_3O_4 nanoparticles shown in the inset of Figure 1a, it is apparent that the minor peak around 9 nm originates from the unloaded Fe_3O_4 nanoparticles. After repeated ultracentrifugation treatment, the size distribution of the sample displays a

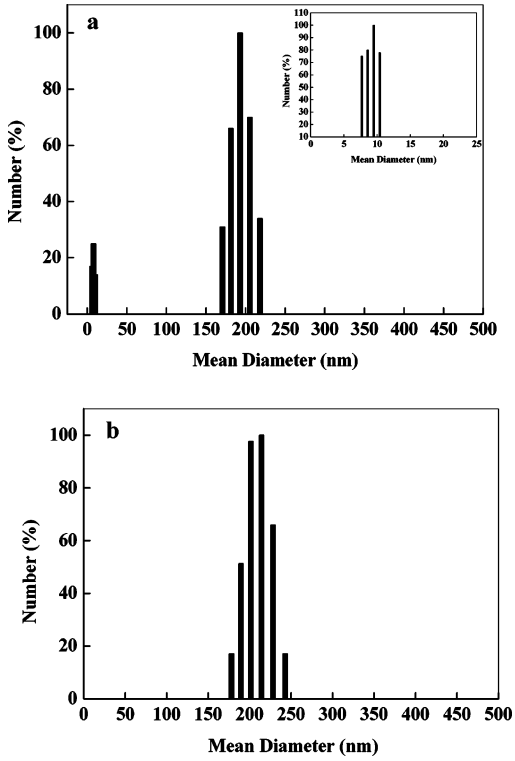

Figure 1. Hydrodynamic diameter D_h distribution of the hybrid spheres: (a) before ultracentrifugation treatment and (b) after treatment. (inset) Size distribution of PVA-stabilized Fe_3O_4 nanoparticles.

unimodal size distribution (Figure 1b) and the hydrodynamic diameter of the hybrid spheres was determined to be 222 ± 18.2 nm, indicating that the unloaded Fe_3O_4 nanoparticles are completely removed after treatment. In addition, a zeta potential measurement of the resulting hybrid spheres showed that the zeta potential of the hybrid spheres was positive and the magnitude was 35.6 ± 2.6 mV, suggesting that chitosan molecules with ionized amino groups were in the outermost layer of the hybrid spheres. Further, the thermogravimetric analysis indicated that the Fe_3O_4 nanoparticles were built into CS−PAA spheres with a loading amount of 8% and an encapsulation efficiency of 57%.

To further characterize the presence of Fe_3O_4 nanoparticles in the CS−PAA spheres after ultracentrifugation treatment and determine the crystallite structure and size of Fe_3O_4 nanoparticles before and after they were built into the spheres, X-ray diffraction patterns were examined for PVA-stabilized Fe_3O_4 nanoparticles and Fe_3O_4 nanoparticle-loaded CS−PAA spheres, as presented in Figure 2. The XRD spectra give a clear crystalline pattern of Fe_3O_4 nanoparticles in both samples.[19] The peak positions of Fe_3O_4 nanoparticles are unchanged before and after incorporation into CS−PAA spheres, but the diffraction intensity of Fe_3O_4 in CS−PAA spheres is lower than that in PVA sample due to lower Fe_3O_4 content. This result suggests that the Fe_3O_4 nanoparticles are indeed incorporated into CS−PAA spheres, and the structure of Fe_3O_4 nanoparticles is not changed during the spheres synthesis process. In addition, trace amounts of hematite (α-Fe_2O_3) and maghemite (γ-Fe_2O_3) are also detected in PVA-stabilized Fe_3O_4 nanoparticles. This may result from oxidation of the iron oxide nanoparticles in air. The average diameter of synthesized Fe_3O_4 nanoparticles was determined to be 8 nm based on the widths of the main peak (311) and a Si standard using the equation[20] $\langle D_{hkl} \rangle = 0.9\lambda/(\beta \cos \theta)$, where $\langle D_{hkl} \rangle$ is the average particle diameter, β is the full-width at half-height of the main peaks, and θ is one-half

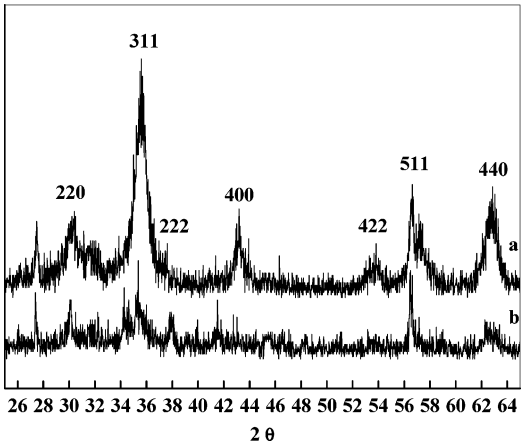

Figure 2. X-ray powder diffraction patterns for (a) PVA-stabilized Fe_3O_4 nanoparticles and (b) Fe_3O_4 nanoparticle-loaded CS−PAA spheres.

the diffraction angle of 2θ. This value is very close to that measured by DSL.

Hybrid Sphere Morphology. Transmission electron microscopy (TEM) was used to characterize the morphology and size of hybrid spheres in the solid state. An intact spherical morphology with an average size of 160 ± 19 nm is observed (Figure 3a). Moreover, no free iron oxide nanoparticles were seen. The salient feature of these hybrid spheres is their hollow interior, as revealed by the TEM image (Figure 3b) obtained by microtoming at room temperature a hybrid sphere sample embedded in epoxy resin. It also noted that no Fe_3O_4 aggregates were observed in the hollow center of cut spheres. However, the electron diffraction pattern (Figure 3c) recorded from the cut sample in Figure 3b and X-ray microanalysis shown in Figure 3d indicate that the Fe_3O_4 nanoparticles are loaded into hollow spheres and located in the wall of the spheres. Figure 4 shows the SEM and AFM images of hybrid hollow spheres. It can be seen in the SEM image that only a very small fraction of spheres shows a partial cave-in or a small opening in their shell wall (Figure 4a), suggesting that the hybrid hollow spheres are permanent shape-persistent when placed under vacuum for SEM observation and the walls of the hollow spheres were structurally robust due to the chemical cross-linking of the CS shell layer using glutaraldehyde. Similarly, the AFM image gives the appearance of the hybrid hollow spheres as the complete spherical shape with an average height of 150 ± 20 nm and an average width of 171 ± 30 nm (Figure 4b). Due to the dry state in microscopic observation, the size observed is smaller than that determined by DLS in aqueous solution.

To understand the possible sites for Fe_3O_4 nanoparticles binding to CS−PAA hollow spheres, FTIR measurements were carried out. The FTIR spectra of CS−PAA spheres, PVA-stabilized Fe_3O_4 nanoparticles, and Fe_3O_4 nanoparticle-loaded CS−PAA spheres are displayed in Figure 5 together with the FTIR spectra of PAA, PVA, and PVA/PAA blend (1:9, wt/wt). It can be seen that for CS−PAA spheres, there are two absorption bands at 1735 and 1633 cm^{-1}, which can be assigned to absorption of C═O groups in PAA and the NH^{3+} group in CS, respectively.[21] The absorption peaks at 1533 cm^{-1} could be assigned to asymmetric stretching vibrations of COO^- anion groups.[21] These results indicate that the carboxylic groups of PAA are dissociated into COO^- groups which complex with protonated amino groups in CS through electrostatic interaction to form the polyelectrolyte complex during the polymerization procedure.[22] For PVA-stabilized Fe_3O_4 nanoparticles, the absorption peaks at 1454 and 1096 cm^{-1} can be assigned to

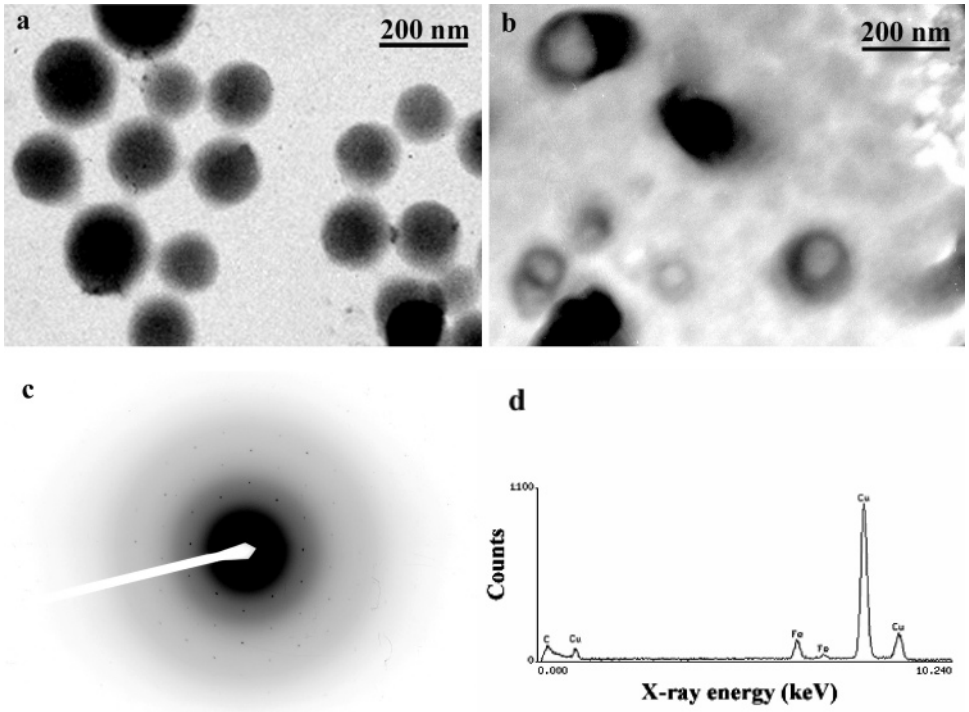

Figure 3. (a) Direct-view TEM image of hybrid spheres. (b) Cut-section TEM image of the hybrid spheres. (c) Electron diffraction of sample shown in b. (d) X-ray energy dispersion spectrum of sample shown in TEM image.

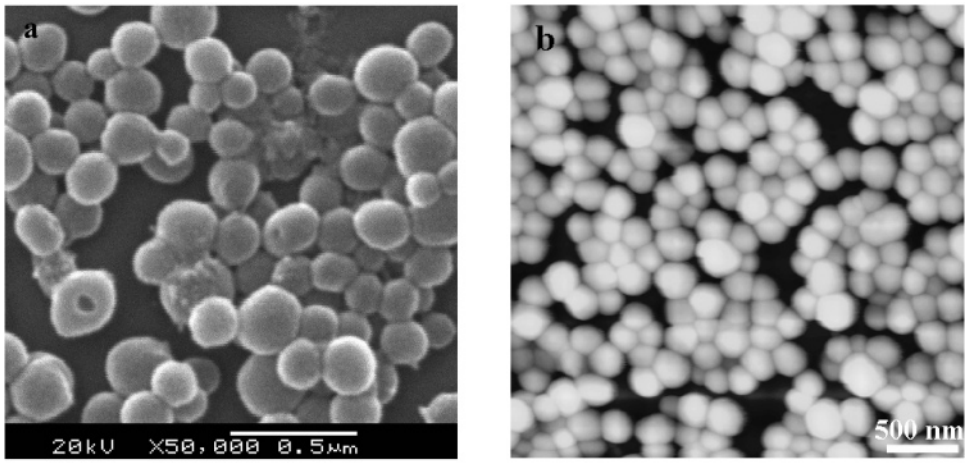

Figure 4. Morphology of hybrid hollow spheres: (a) SEM image and (b) AFM image.

bending vibrations of C−H bonds and stretching vibrations of C−O bonds of PVA, respectively, while the absorption peak at 583 cm^{-1} can be ascribed to Fe_3O_4. However, compared to the FTIR spectrum of CS−PAA spheres, the absorption peak of the carboxyl groups of PAA at 1735 cm^{-1} shifts to 1716 cm^{-1} and the absorption peak of COO^- in PAA at 1533 cm^{-1} shifts to 1506 cm^{-1} for Fe_3O_4 nanoparticle-loaded CS−PAA spheres, suggesting formation of intermolecular hydrogen bonds between PAA and PVA. This is confirmed by the FTIR spectrum of PAA/PVA blend (Figure 5b). It is found that the absorption peak of the carboxyl group in PAA mainly occurs at 1713 cm^{-1} in the blend of PAA and PVA. Thus, incorporation of PVA-stabilized Fe_3O_4 nanoparticles into the CS−PAA hollow spheres is mainly achieved by interaction between PAA and PVA attached to Fe_3O_4 nanoparticles. It is also demonstrated that the Fe_3O_4 nanoparticles are mainly located in the inner shell of the hybrid hollow spheres since the PAA is in the inner shell of the CS−PAA hollow spheres, as shown in the high-resolution TEM image.[15]

In our previous work[22] we found that CS could interact with monomer AA, and this interaction induced the formation of core−shell structure micelles with positively charged protonated CS chains as the shell and the polyion complexes of CS and AA (i.e., positively charged protonated CS chains and negatively charged dissociated acrylic acid) as the core. When AA monomers were polymerized in aqueous solution, the hollow polymeric nanospheres were spontaneously formed. In the present case, a reasonable speculation is that addition of PVA-stabilized Fe_3O_4 nanoparticle does not change the formation mechanism of CS−PAA hollow spheres. Since there is an interaction between PVA and PAA, the PVA-stabilized Fe_3O_4 nanoparticles should be incorporated into the inner shells of spheres where polyelectrolyte complex between CS and PAA exists. Cavity formation in the center of the hybrid spheres can be ascribed to the force balance between an electrostatic attraction force in CS and PAA drawing spheres shrinkage and an electrostatic repulsion force from the positive charges in the shell, which trends to expand the spheres.

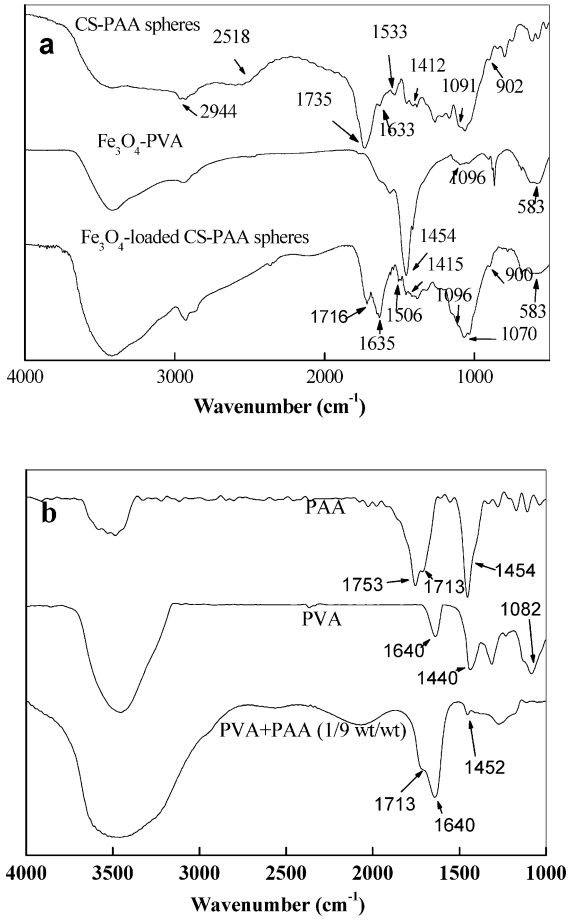

Figure 5. (a) FT-IR spectra of CS−PAA hollow spheres, PVA-stabilized Fe_3O_4 nanoparticles, and hybrid CS−PAA hollow spheres. (b) FT-IR spectra of PAA, PVA, and the blend of PAA and PVA (PAA/PVA = 9/1 wt/wt).

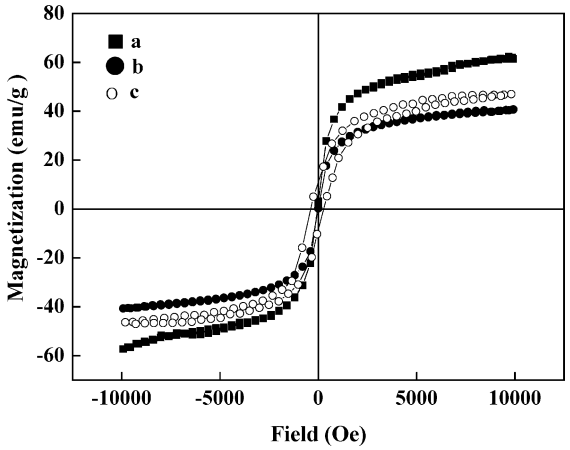

Figure 6. Magnetization versus applied magnetic field: (a) PVA-stabilized Fe_3O_4 nanoparticles at room temperature and (b and c) hybrid hollow spheres at room temperature and 78 K, respectively.

Magnetic Properties. The magnetic properties of the hybrid hollow spheres were measured by vibrating sample magnetometry (VSM). Field-dependence hysteresis loops of PVA-stabilized Fe_3O_4 nanoparticles and hybrid CS−PAA hollow spheres are presented in Figure 6. The magnetization values were normalized to the Fe_3O_4 content in the samples. From Figure 6 it can be seen that the hysteresis and coercivity are almost undetectable, suggesting that the PVA-stabilized Fe_3O_4 nanoparticles and hybrid hollow spheres have superparamagnetic properties at room temperature. As the temperature is significantly lowered to 78 K, the hybrid hollow spheres exhibit a hysteresis with coercivity of 400 Oe, indicating that the hollow hybrid spheres show ferrimagnetic characteristics at this temperature. The saturation magnetizations of PVA-stabilizing Fe_3O_4 nanoparticles and hybrid CS−PAA hollow spheres at room temperature are 62.3 and 40.7 emu/g, respectively, which are lower than that of the bulk Fe_3O_4 (89 emu/g).[23] The loss of magnetization can be attributed to the small particle size effect since a noncollinear spin arrangement occurs primarily at or near the surface.[24−26] The difference in magnetization value between PVA-stabilized Fe_3O_4 nanoparticles and hybrid CS−PAA hollow spheres can be attributed to the nonmagnetic organic components which also can reduce the total magnetization to a different extent.[26]

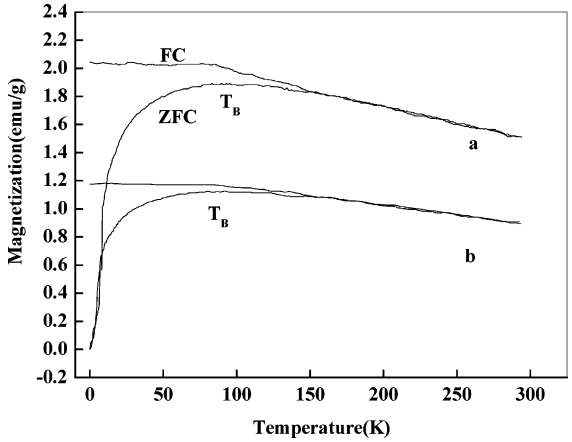

Figure 7. Field-cooled (FC) and zero-field-cooled (ZFC) magnetization curves of the PVA-stabilized Fe_3O_4 nanoparticles (a) and hybrid hollow spheres (b). In the field cooling the applied field was 200 Oe.

Field-cooled (FC) and zero-field-cooled (ZFC) magnetization curves of the PVA-stabilized Fe_3O_4 nanoparticles and hybrid hollow spheres are displayed in Figure 7. The applied field was 200 Oe in the case of the field-cooling experiment. Both samples exhibited the same trend in FC and ZFC curves, and a maximum in the ZFC curve was observed. This maximum is normally taken as indicative of a spin glass state where weak local anisotropy would destroy the long-range magnetic order, giving rise to formation of a glasslike phase at high temperature.[27] Additionally, the effects of the temperature dependence of the reorientation of the magnetic moment associated to the magnetic nanoparticle, saturation magnetization, and magnetic anisotropy were also proposed to explain the behavior of magnetic nanoparticles in ZFC curve.[28] The blocking temperatures (corresponding to the maximum in the ZFC curve) for PVA-stabilized Fe_3O_4 nanoparticles and hybrid hollow spheres are 80 and 87 K, respectively, indicating that the size of Fe_3O_4 nanoparticles does not increase significantly after they are built into CS−PAA spheres.

Since Mössbauer spectroscopy is particularly sensitive in the system where the iron oxide is relatively low in concentration or crystalline, the hybrid CS−PAA hollow spheres were further investigated using Mössbauer spectroscopy. Figure 8 shows the Mössbauer spectrum of hybrid CS−PAA hollow spheres at room temperature (298 K) in the absence of an external magnetic field. From the Mössbauer spectrum, superposition of a central quadrupole doublet and a magnetic split which broadens the adsorption in the background was observed. Fitting the spectrum gave rise to a doublet with an isomer shift of 0.39 mm/s and quadrupolar splitting of 0.29 mm/s and a sextet with an isomer shift of 0.32 mm/s. It is known that at a certain temperature the parameters of the doublet and sextet are typical for a super-

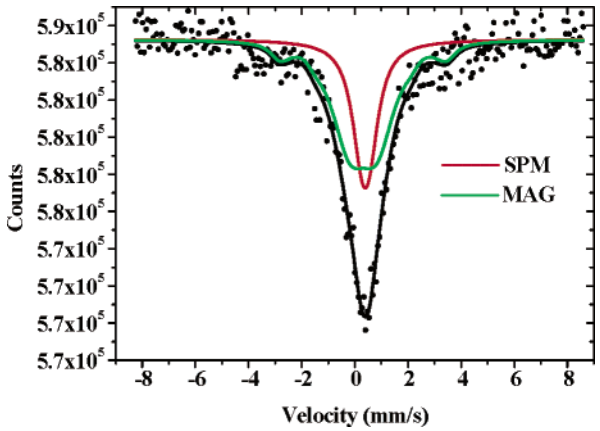

Figure 8. Mössbauer spectrum of hybrid hollow spheres at room temperature in the absence of an external magnetic field. The red and green curves indicate deconvoluted superparamagnetic and magnetic components of the fitting of the Mössbauer spectrum, respectively.

paramagnetic (SPM) and magnetic split, respectively.[29] For a given particle size, the Mössbauer spectrum will be magnetically split below the so-called blocking temperature T_B. Above T_B it will collapse into the paramagnetic spectrum. The fraction of iron oxide nanoparticles undergoing superparamagnetic and magnetic split in hybrid hollow spheres, as estimated from the area of the doublet and sextet, is about 35% and 65%, respectively. On the basis of an approximate expression for the blocking diameter at temperature T[30]

$$d_b = \left[\frac{6}{\pi}\frac{k_B T}{K}\ln\frac{\upsilon_0}{\upsilon_L}\right]\frac{1}{3}$$

where k_B and K is the Boltzmann constant and anisotropy constant of the material, respectively, υ_0 is an attempt frequency on the order of $10^{10}-10^{11}s^{-1}$, and υ_L is the Mössbauer hyperfine Larmor frequency of 50 MHz for ^{57}Fe, we obtained a d_b value of around 9.4 nm using $K = 5 \times 10^4$ J/m^3.[31] This means that at room temperature the iron oxide nanoparticles with a size of larger than 9.4 nm will yield a magnetic split while the smaller iron oxide nanoparticles remain in the superparamagnetic relaxation state. Thus, the appearance of hyperfine magnetic structure in the Mössbauer spectrum at room temperature can be explained by the presence of large-sized Fe_3O_4 nanoparticles (larger than 9 nm) in the sample as seen in the size distribution of Fe_3O_4 nanoparticles in the inset of Figure 1a. Another contribution to the formation of magnetic split in the Mössbauer spectrum may be the chains (or islands) of interacting iron oxide nanoparticles generated in the confined sphere wall (possibly by means of dipole−dipole interaction[32]) since such chains consisting of iron oxide nanoparticles in the sphere wall have been directly observed by TEM in the Fe_3O_4−nanoparticle-loaded polymeric hollow nanospheres with a size of 65 nm.[15] In addition, the difference in the magnetic property that we observed in the VSM and Mössbauer spectrum indicates that Mössbauer spectroscopy is more effective in observing the hyperfine magnetic structure of samples.

Since superparamagnetic Fe_3O_4 nanoparticles are T2-type contrast agents in MRI imaging and CS is a biocompatible and biodegradable macromolecule, it is interesting to know if Fe_3O_4 nanoparticle-loaded CS−PAA hollow spheres have a magnetic resonance (MR) signal-enhanced property. To know this, a phantom test was carried out. Figure 9 shows a T2-weighted MR image of hybrid CS−PAA hollow spheres with various concentrations in water. It can be seen that the MR signal

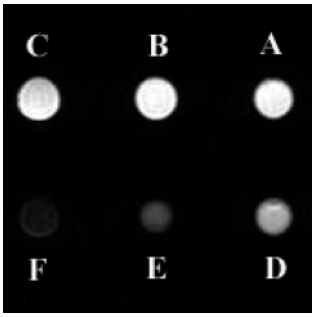

Figure 9. T2-weighted MR image with the various concentrations (c) of hybrid hollow spheres in water: (a) water, (b) $c = 0.35$ g/L, (c) $c = 0.7$ g/L, (d) $c = 1.4$ g/L, (e) $c = 3.5$ g/L, and (f) $c = 7.0$ g/L.

intensity (related to the T2 relaxation time in T2-weighted image) for the different concentration samples is not identical. With increasing hybrid hollow sphere concentration in water, the MR signal is enhanced significantly (negative in brightness in T2-weighed image). This result indicates that the hybrid hollow sphere can generate high magnetic field gradients near the surface of the hybrid spheres, and the signal can be detected using the spin−echo technique with TR/TE = 3000 ms/80 ms even at very low sphere concentrations.

Conclusions

We demonstrate a novel approach to produce hybrid hollow spheres starting with the PVA-stabilized Fe_3O_4 nanoparticles and a water-soluble polymer−monomer pair between a biopolymer (CS) with amino groups and organic monomers (AA) with acid groups. This approach gives the hybrid hollow spheres a functional surface with chemical groups for subsequent chemical reactions.

In addition, this synthesis methodology provides a new route for the encapsulation of functional materials with larger size (for example, larger than a macromolecular size). It is also possible to extend this approach to other systems in which a weak interaction between polymer and monomer, such as acid−base, electrostatic and hydrogen bond, is present.

Acknowledgment. This work is supported by the Natural Science Foundation of China (20374026 and 10334020), the 973 Program of MOST (2003CB615600), and the Natural Science Foundation of Jiangsu Province, China (BK2001029).

References and Notes

(1) (a) Meier, W. *Chem. Soc. Rev.* **2000**, *29*, 295. (b) Ameller, T.; Marsaud, W.; Legrand, P.; Gref, R.; Renoir, J. M. *Int. J. Cancer* **2003**, *106*, 446.
(2) (a) Tartaj, P.; Morales, M. P.; Veintemillas-Verdaguer, S.; Gonzalez-Carreno, T.; Serna, C. J. *J. Phys. D: Appl. Phys.* **2003**, *36*, R182. (b) Marinakos, S. M.; Anderson, M. F.; Ryan, J. A.; Martin, L. D.; Feldheim, D. L. *J. Phys. Chem. B* **2001**, *105*, 8872.
(3) (a) Zhong, Z. Z.; Yin, Y. D.; Gates, B.; Xia, Y. *Adv. Mater.* **2000**, *12*, 206. (b) Tissot, I.; Reymond, J. P.; Lefebvre, F.; Bourgeat-Lami, E. *Chem. Mater.* **2002**, *14*, 1325. (c) Imhof, A. *Langmuir* **2001**, *17*, 3579. (d) Shiho, H.; Kawahashi, N. *Colloid Polym. Sci.* **2000**, *278*, 270. (e) Sertchook, H.; Avnir, D. *Chem. Mater.* **2003**, *15*, 1690.
(4) (a) Caruso, F.; Caruso, R. A.; Mohwald, H. *Science* **1998**, *282*, 1111. (b) Kawahashi, N.; Matijevic, E. *J. Colloid Interface Sci.* **1990**, *138*, 534. (c) Caruso, F.; Spasova, M.; Susha, A.; Giersig, M.; Caruso, R. A. *Chem. Mater.* **2001**, *13*, 109.
(5) Wong, M. S.; Cha, J. N.; Choi, K. S.; Deming, T. J.; Stucky, G. D. *Nano Lett.* **2002**, *2*, 583.
(6) Cha, J. N.; Birkedal, H.; Euliss, L. E.; Bartl, M. H.; Wong, M. S.; Deming, T. J.; Stucky, G. D. *J. Am. Chem. Soc.* **2003**, *125*, 8285.
(7) Du, J.; Chen, Y. *Macromolecules* **2004**, *37*, 5710.

(8) Strohm, H.; Sgraja, M.; Bertling, J.; Lobmann, P. *J. Mater. Sci*. **2003**, *38*, 1605.
(9) Shchukin, D. G.; Radtchenko, I. L.; Sukhorukov, G. B. *Mater. Lett.* **2003**, *57*, 1743.
(10) Ugelstad, J.; Berge, A.; Ellingsen, T.; Schmid, R.; Nilsen, T. N.; Mork, P. C.; Stenstad, P.; Hornes, E.; Olsvik, O. *Prog. Polym. Sci.* **1992**, *17*, 87.
(11) Nakayama, H.; Arakaki, A.; Maruyama, K.; Takeyama, H.; Matsunage, T. *Biotechnol. Bioeng.* **2003**, *84*, 96.
(12) Jia, H. F.; Zhu, G. Y.; Wang, P. *Biotechnol. Bioeng.* **2003**, *84*, 406.
(13) Billotey, C.; Wilhelm, C.; Devaud, M.; Bacri, J. C.; Bittoun, J.; Gazeau, F. *Magn. Reson. Med.* **2003**, *49*, 646.
(14) Patil, G. V. *Drug. Dev. Res*. **2003**, *58*, 219.
(15) Ding, Y.; Hu, Y.; Jiang, X.; Zhang, L.; Yang, C. *Angew. Chem., Int. Ed*. **2004**, *46*, 6369.
(16) Lee, J.; Isobe, T.; Senna, M. *J. Colloid Interface Sci*. **1996**, *177*, 490.
(17) Dan, Y.; Chen, S. Y.; Zhang, Y. F.; Xiang, F. R. *J. Polym. Sci., B: Polym. Phys.* **2000**, *38*, 1069.
(18) Hu, Y.; Chen, Y.; Chen, Q.; Zhang, L.; Jiang, X.; Yang, C. *Polymer* **2005**, *46*, 12703.
(19) *JSPDS Data Cards*; International Center of Diffraction Data: Swarthmore, PA, 1988.
(20) Cornell, R. M.; Schwertmann, U. *The Iron Oxide*; VCH: Weinheim, 1996.
(21) Hu, Y.; Jiang, X.; Ding, Y.; Ge, H. X.; Yuan, Y. Y.; Yang, C. Z. *Biomaterials* **2002**, *23*, 3193.
(22) Hu, Y.; Jiang, X.; Ding, Y.; Chen, Q.; Yang, C. *Adv. Mater.* **2004**, *16*, 933.
(23) Landfester, K.; Ramírez, L. P. *J. Phys.: Condens. Matter*. **2003**, *15*, S1345.
(24) Morales, M. P.; Verdaguer, S. V.; Montero, M. I.; Sterna, C. J.; Roing, A.; Casas, L.; Martinez, B.; Sandiumenge, F. *Chem. Mater.* **1999**, *11*, 3058.
(25) Morup, S.; Bodker, F.; Hendriksen, P. V.; Linderoth, S. *Phys. Rev. B* **1995**, *52*, 287.
(26) Shafi, K. V. P. M.; Ulman, A.; Dyal, A.; Yan, X.; Yang, N.-L.; Estournes, C.; Fournes, L.; Wattiaux, A.; White, H.; Rafailovich, M. *Chem. Mater.* **2002**, *14*, 1778.
(27) Kenning, G. G.; Chu, D.; Orbach, R. *Phys. Rev. Lett.* **1991**, *66*, 2923.
(28) Morais, P. C.; Teixeira, C. B.; Neto, K. S.; Azevedo, R. B.; Lacava, Z. G. M.; Lacava, L. M. *Solid State Commun.* **2000**, *114*, 59.
(29) Mikhaylova, M.; Kim, D. K.; Bobrysheva, N.; Osmolowsky, M.; Semenov, V.; Tsakalakos, T.; Muhammed, M. *Langmuir* **2004**, *20*, 2472.
(30) Bean, C. P.; Livingston, J. D. *J. Appl. Phys.* **1959**, *30*, 120S.
(31) Pinna, N.; Grancharov, S.; Beato, P.; Bonville, P.; Antonietti, M.; Niederberger, M. *Chem. Mater.* **2005**, *17*, 3044.
(32) Novakova, A. A.; Lanchinskaya, V. Yu.; Volkov, A. V.; Gendler, T. S.; Kiseleva, T. Yu.; Moskvina, M. A.; Zezin, S. B. *J. Magn. Magn. Mater.* **2003**, *258*−*259*, 354.

BM060085H